# Sn-catalyzed synthesis of $SnO_2$ nanowires and their optoelectronic characteristics

Nanotechnology **22** (2011) 485701 (7pp) doi:10.1088/0957-4484/22/48/485701

# Sn-catalyzed synthesis of $SnO_2$ nanowires and their optoelectronic characteristics

**Lin-bao Luo[1], Feng-xia Liang[2] and Jian-sheng Jie[1]**

[1] School of Electronic Science and Applied Physics, Hefei University of Technology, Hefei, Anhui 230009, People's Republic of China
[2] Department of Physics and Materials Science, City University of Hong Kong, Hong Kong SAR, People's Republic of China

E-mail: luolb@hfut.edu.cn and jsjie@hfut.edu.cn

Received 24 August 2011, in final form 3 October 2011
Published 4 November 2011
Online at stacks.iop.org/Nano/22/485701

**Abstract**

We report the rational synthesis of one-dimensional $SnO_2$ nanowires ($SnO_2$NWs) via a Sn-catalyzed vapor–liquid–solid (VLS) growth mechanism, in which Sn nanoparticles can direct the oriented growth of $SnO_2$NWs at high temperature. $I$–$V$ measurement of a field effect transistor made of individual $SnO_2$NWs exhibits typical n-type semiconducting characteristics with an electron mobility and concentration of 14.36 $cm^2\ V^{-1}\ s^{-1}$ and $1.145 \times 10^{17}\ cm^{-3}$, respectively. The $SnO_2$NW-based photodetector shows a high sensitivity to UV light radiation, and a fast light response speed of millisecond rise time/fall time with excellent stability and reproducibility, whereas it is nearly blind to illumination with wavelengths in the visible range. Detailed reasons to account for the detection selectivity and rapid response speed are proposed. The generality of the above results suggests that our $SnO_2$NW photodetectors have potential application in nanoscaled optoelectronic devices.

(Some figures may appear in colour only in the online journal)

## 1. Introduction

One-dimensional (1D) metal oxide semiconductor nanostructures, including nanotubes, nanowires and nanoribbons, are very attractive and promising building blocks for future electronic systems by virtue of the unique possibilities they offer for the rational control of fundamental properties such as chemical composition, dimension, and doping level during growth [1, 2]. So far a huge number of nanostructures have been successfully synthesized using approaches ranging from laser-ablation [3] and thermal evaporation [4], to microwave radiation processes and solution-phase growth [5, 6]. Structural characterization of these semiconducting nanostructures and exploration of their novel device applications have been well documented [7–9].

Tin dioxide ($SnO_2$) with a wide band gap ($E_g$ = 3.6 eV at 300 K) is a stable, environmentally friendly semiconductor, which is well known for its wide range of applications, e.g., in dye-sensitized solar cells [10], transparent conducting electrodes [11], catalyst supports [12], and so on. $SnO_2$ nanostructures in low-dimensional form prepared from sol–gel [13], magnetron sputtering [14], chemical vapor deposition [15], pulsed delivery [16] and hydrothermal and thermal evaporation [17, 18] have shown novel optical and electrical characteristics that are different from their thin film and bulk counterparts [19, 20]. By this token, 1D nanostructured $SnO_2$ including nanowires, nanoribbons and nanobelts has found applications in chemical sensors [21, 22], field effect transistors (FETs), light emitting diodes (LEDs), etc [23]. To date, while various ultraviolet (UV) light photodetectors have been successfully fabricated from ZnO nanowires [24], GaN nanowires [25] and carbon nanotubes [26], comparatively little work has been carried out to study $SnO_2$ nanowire ($SnO_2$NW)-based UV light photodetectors [27–29]. Consequently, their photoconductive properties such as illumination spectral response, illumination intensity response and response speed are underdeveloped. Exploration along this direction is highly desirable as it is not only helpful for understanding the light detection mechanism, but also beneficial to the development of high-performance nanodevices which may find application in future optoelectronic circuits, imaging techniques and light-wave communications. In this work, we present an approach to the synthesis of $SnO_2$NWs via a Sn-catalyzed growth

 

mechanism. The as-prepared $SnO_2$NWs exhibit typical n-type electrical conduction characteristics. Notably, the individual $SnO_2$NW-based photodetector shows high sensitivity to UV light illumination with high response rate and excellent reproducibility.

## 2. Experimental section

### *2.1. Synthesis of $SnO_2$ NWs and their structural study*

The synthesis of $SnO_2$NWs was carried out in a horizontal tube furnace. Briefly, $SnO_2$ power (analytical grade, Sigma-Aldrich Co.) was placed at the center of the alumina tube, silicon substrates were placed in a downstream position from the source material (∼17 cm). After the tube was evacuated to a base pressure of $10^{-4}$ Torr, the source was heated up to 1050 °C at a rate of 20 °C $min^{-1}$ and then was maintained at this temperature for 2–4 h. During the growth process, a carrier gas of high-purity argon premixed with 5% hydrogen was fed at a total flow rate of 20 sccm. The phase, morphology and structure of the as-prepared light yellow $SnO_2$NWs were characterized using an x-ray diffractor (XRD, Siemens D-500 using Cu K$\alpha$ radiation), field emission scanning electron microscopy (FESEM, Philips XL 30 FEG), transmission electron microscopy (TEM, Philips CM 20, operated at 200 kV) attached with energy-dispersive x-ray spectroscopy (EDX), and high-resolution transmission electron microscopy (HRTEM, Philips CM 200 FEG, operated at 200 kV). The chemical composition of the product was analyzed by x-ray photoemission spectroscopy (XPS) which was performed on a VG ESCALAV 220i-XL surface analysis system equipped with a monochromatic Al K$\alpha$ x-ray (1486.6 eV) source.

### *2.2. Device fabrication*

The fabrication processes of both FET and UV light photodetector devices are identical. Briefly, $p^+$-Si substrates were cut into small pieces with areas of 1.5 × 1.5 $cm^2$, and were washed stepwise with absolute alcohol and distilled water under ultrasonication for 10 min, respectively. A layer of 100 nm thick $Si_3N_4$ film as dielectric layer was then coated by using a magnetron sputtering system. Afterward, on the $Si_3N_4$ layer, $SnO_2$NWs were dispersed with the desired density. Finally, a photolithography technique (mask aligner: Karl Suss MJB-3) was used to define both the source and the drain electrodes, and an ultra-high vacuum electron-beam evaporator was employed to form both the source and the drain electrodes by depositing a mixed Ti/Au (20/50 nm) layer.

### *2.3. Device characterization*

A two-probe configuration method was employed throughout this work. A light system including a xenon lamp (150 W) and a monochromator ($\frac{1}{8}$, Spectra-physics 74 000) was used to provide the monochromatic light, which was focused and guided perpendicularly onto the nanowires by a quartz lens. Electrical measurements were carried out on the semiconductor characterization system (4200-SCS, Keithley Co.) with picoampere resolution. Unless stated, all electrical measurements were carried out at room temperature. To measure the time response of the NWs to pulsed light radiation, a mechanically rotating chopper operated at a frequency of 0–500 Hz was used to automatically switch on and off the incident UV light. During measurement, the time-variation of the photocurrent was collected by an oscilloscope system (Infiniium, Agilent Co.).

## 3. Results and discussion

### *3.1. Morphology and structure analysis*

The $SnO_2$NWs were synthesized via thermal evaporation of pure tin oxide powder in $N_2/H_2$ atmosphere. The as-collected NW on Si wafer was then directly transferred into the FESEM chamber for morphology characterization. As shown in figure 1(a), the silicon substrate was fully covered by a high density of wire-like nanostructures with lengths of several micrometers. EDS analysis revealed that the product was mainly composed of Sn and O elements, accounting for 42.6 and 57.4% (atomic ratio), respectively. The presence of both Sn and O was also confirmed by the x-ray powder diffraction (XRD) study. Figure 1(b) shows a typical diffraction pattern, in which the peaks labeled with stars can be readily indexed to the tetragonal rutile-phase of $SnO_2$ (JCPDS card No. 41-1445), with lattice constants of $a = b = 0.474$ nm and $c = 0.319$ nm which are consistent with the literature values [30, 31]. Additionally, typical peaks due to Sn phase (JCPDS card No. 04-0673) were also present in the pattern (labeled with #) [32]. The XPS spectrum of the $SnO_2$NWs in figure 1(c) further reveals the presence of both Sn (486 eV) and O (533 eV). Deconvolution of the asymmetrical peak in the range of 480–495 eV gives rise to two separate ones, which can be readily assigned to the Sn $3d_{5/2}$ for Sn(0) and Sn(IV), respectively.

TEM was employed to study the crystal structure of the $SnO_2$NWs (figures 2(a), (b) and (e)). Evidently, one can see that the diameters of the as-prepared NWs are in the range from 40 to 80 nm. Interestingly, there is at least one black nanoparticle on the head of each $SnO_2$NW, as shown in the TEM images. The distinct contrast difference between the tip and the stem of the NWs suggests that they may consist of different materials. Indeed, these tips, according to comparative EDS analysis of both parts A and B in figures 2(c) and (d), are largely composed of tin atoms. The upper inset SAED pattern shown in figure 2(e) was recorded on an individual NW with the electron beam along the [001] zone axis, indicating the single-crystalline nature of the $SnO_2$NW. The lattice fringes in the HRTEM image further confirm the single-crystal characteristics of the NWs. The $d$-spacing (0.33 nm) between adjacent lattice planes corresponds to the [110] growth direction of the $SnO_2$NWs [33].

It has been demonstrated that Sn nanoparticles can effectively catalyze the oriented growth of 1D ZnO [34], $SiO_2$ [35], and Si nanowires [36, 37] via a vapor–liquid–solid (VLS) mechanism. Similarly, the formation of $SnO_2$NWs in this study can also be explained by a Sn-catalyzed growth model illustrated in figure 3. At high temperature, $SnO_2$

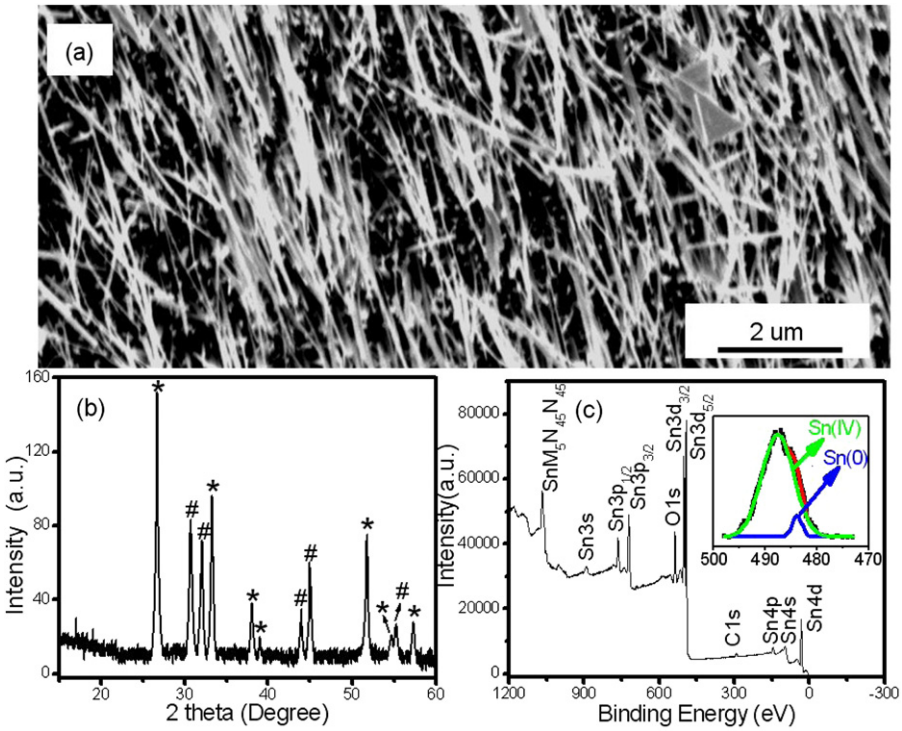


**Figure 1.** (a) FESEM images of the as-produced $SnO_2$NWs. (b) XRD pattern of the $SnO_2$NWs. (c) XPS spectrum of the $SnO_2$NWs. The inset shows the Sn $3d_{5/2}$ spectrum at higher resolution.

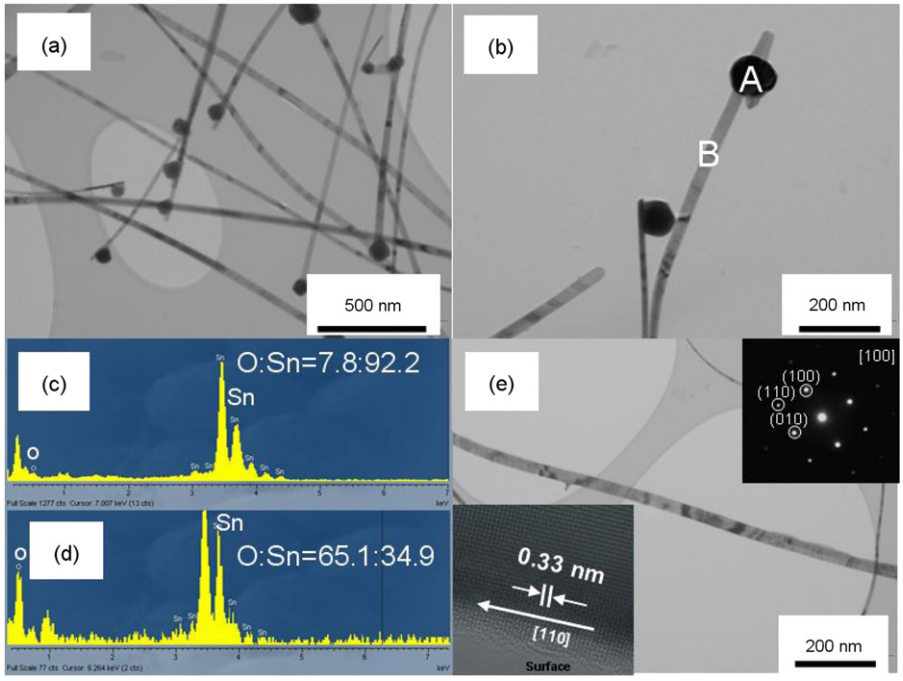


**Figure 2.** (a) A typical bright-field TEM image of $SnO_2$NWs at low magnification. (b) A typical bright-field TEM image of $SnO_2$NWs with a Sn tip. (c), (d) EDX analysis of parts A and B, respectively, shown in (b). (e) TEM image of the stem of a typical $SnO_2$NW. The lower inset shows the HRTEM of a $SnO_2$NW with growth orientation along [110], the upper inset is the corresponding SAED pattern.

firstly sublimes to form highly reactive $SnO_2$ vapor which is then reduced by $H_2$ gas through the following chemical equation: $SnO_2$ (g) + $2H_2$ (g) → Sn (g) + $2H_2O$ (g). The resulting Sn nanoparticles can act as effective catalysts to dissolve $SnO_2$, leading to the formation of $SnO_2$–Sn eutectic alloy droplets. Due to its relative high melting point (1627 °C), $SnO_2$ can easily precipitate out of the supersaturated droplet, giving rise to growth in an oriented way. Note that the above

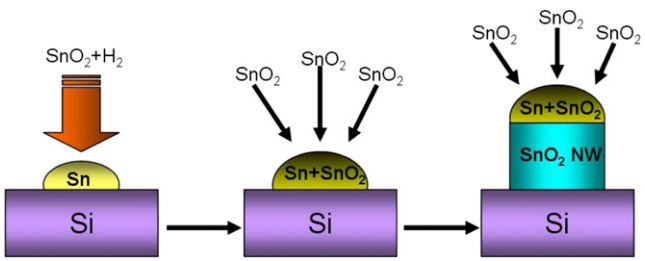


**Figure 3.** Schematic illustration of $SnO_2$NW growth via the VLS mechanism. This reaction is catalyzed by Sn–$SnO_2$ eutectic alloy droplets deposited on the silicon wafer surface.

chemical reaction process can take place spontaneously at high temperature (927 °C) as the difference of Gibbs free energy ($-296.95$ kJ mol$^{-1}$) is less than 0 [38].

### 3.2. Field effect transistor characterization

To evaluate the electrical property of the as-prepared $SnO_2$NWs, a metal insulator semiconductor field effect transistor (MISFET, the nanodevice configuration is schematically illustrated in the inset to figure 4(a)) was fabricated. Figure 4(a) shows the gate-dependent current versus bias voltage curves, in which all the $I$–$V$ curves are linear, signifying that perfect contact (Ohmic contact) was formed between the Ti/Au electrodes and the $SnO_2$NWs. Moreover, the decrease of electrical conduction with gate voltage reveals the typical characteristics of the $SnO_2$NW-FET with an n-type channel. Figure 4(b) plots typical transfer curves at $V_{ds} = 0.1$ V from the same device. By fitting the linear part of the $I_{ds}$–$V_g$ curve, the turn-on threshold voltage ($V_T$) and transconductance ($g_m = dI_{ds}/dV_g$) are estimated to be $-7.5$ V, and 28.4 nS, respectively. Additionally, the electron mobility ($\mu_e$) can be determined from the relation: $g_m = \mu_e C V_{ds}/L^2$, where $L$ is the length of the $SnO_2$NW (2.3 $\mu$m) and $C$ is the channel capacitance which can be described by the formula of $C = 2\pi\varepsilon_0\varepsilon_{r,\mathrm{eff}}L/\cosh^{-1}(t/r)$ assuming a cylinder on an infinite plate model for the $SnO_2$NW based MISFET, where $\varepsilon_{r,\mathrm{eff}}$ is the effective dielectric constant for $Si_3N_4$(7.5), $t$ is the distance between the $p^+$-Si substrate and the center of the NW (100 nm), and $r$ is the radius of the NW (80 nm). On the basis of the above constants, $\mu_h$ is calculated to be 14.36 cm$^2$ V$^{-1}$ s$^{-1}$, which is comparable with the literature value [39]. What is more, the electron concentration ($n_h$) is estimated to be $1.145 \times 10^{17}$ cm$^{-3}$ from the relation $n_h = 1/\rho q \mu_h$, where $\rho$ (the resistivity of the $SnO_2$NW) is 3.01 Ω cm, according to $\rho = R\pi r^2/L$. In addition to the parameters mentioned above, a subthreshold swing (SS) of $7.29 \times 10^2$ mV/dec is derived from the relation $S = \ln(10)[dV_g/d(\ln I_{ds})]$. Significantly, this value is nearly comparable with that of Ta-doped $SnO_2$NWs [27], and only one order of magnitude higher than the theoretical limit value ($S \approx 60$ mV/dec) that can be determined from the formula $S = \ln(10)(k_B T/e)$, where $k_B$ is Boltzmann's constant, $T$ is the absolute temperature and $e$ is the elementary charge [40]. This relatively low subthreshold swing confirms that the $SnO_2$NWs are suitable for transistor applications.

### 3.3. Photoconductive property

When the individual $SnO_2$NW-based devices were illuminated with UV light, they showed remarkable photoconductive characteristics. As observed from figure 5(a), the electrical current increased dramatically and stabilized at a high-conduction 'on' state upon light radiation, but it decreased quickly to a low-conductivity 'off' state after the UV light was switched off, leading to an on/off ratio as high as $10^3$. Further spectral photoresponse study reveals that the photoconductive behavior is highly dependent on the wavelength of the incident light. Figure 5(b) depicts the $I$–$V$ curves measured under light illumination with different wavelengths. To make this analysis more reliable, the light intensity was kept the same during the spectral response study. It is visible that the $SnO_2$NW exhibits high sensitivity to UV light illumination with a sensitivity edge at about 340 nm, corresponding closely to the energy gap of 3.6 eV derived from the UV–vis absorption curve (inset to figure 5(b)). This agreement is believed to be highly associated with the photoconductive mechanism. That is, the photoresponse of the semiconductor nanostructures to light radiation is in fact a result of a complex process of electromagnetic radiation absorption, carrier generation, trapping, and recombination [41]. Upon ultraviolet illumination, the photoenergy of 320 nm UV light

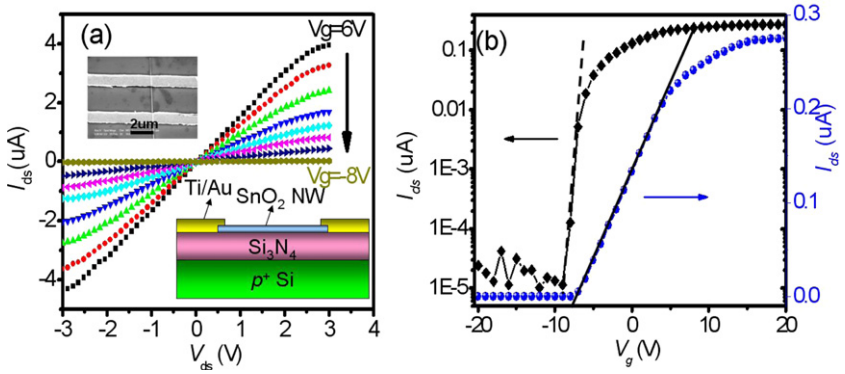


**Figure 4.** (a) $I_{ds}$–$V_{ds}$ curves of the $SnO_2$NW-FET measured for different gate voltages. $V_g$ increases from $-8$ to 6 V in steps of 2 V. The lower inset shows a schematic illustration of the $SnO_2$NW-based FET, the upper inset shows an SEM image of the FET device. (b) $I_{ds}$ versus $V_g$ curve recorded at $V_{ds} = 0.1$ V.

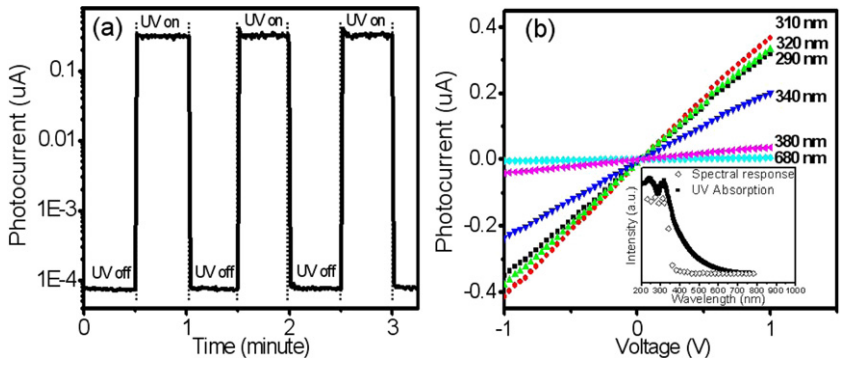


**Figure 5.** (a) Photocurrent versus time recorded with the 2 mW cm$^{-2}$ UV light illumination switched on and off repeatedly. The wavelength of the incident light is 320 nm. During measurement, $V_{ds}$ is kept at 1 V. (b) $I$–$V$ curves of a single $SnO_2$NW under 2 mW cm$^{-2}$ UV light illumination with different wavelengths. The inset shows the spectral photoresponse and UV–visible spectrum within 200–800 nm wavelengths.

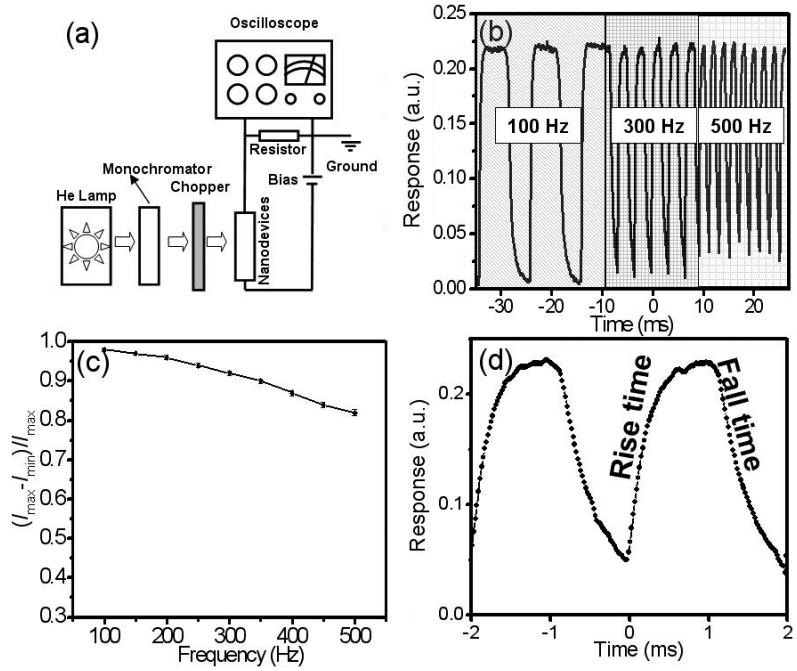


**Figure 6.** (a) Schematic diagram of the photoresponse measurement setup. (b) Photoresponse of the $SnO_2$NW photodetector to the pulsed incident light at frequencies of 100, 300 and 500 Hz (320 nm, 2 mW cm$^{-2}$). During measurement, the bias voltage was kept at 3 V. (c) $(I_{max} - I_{min})/I_{max}$ versus the frequency of the pulsed UV light. (d) Photoresponse of the photodetector at a frequency of 500 Hz.

(3.87 eV) is sufficient to lift electrons directly from the valence band to the conduction band in the $SnO_2$NWs, whose band gap is around 3.6 eV, by extrapolating the UV–vis adsorption spectrum. Photons with insufficient energy cannot excite electrons from the valence band to the conduction band and thus do not contribute to the photocurrent. It is worth noting that although high energy photon is indispensable for photoconductivity it does not necessarily lead to high responsivity. A case in point is the reduced photocurrent for 290 nm light, as observed in figure 5(b). This slight drop in sensitivity to UV light with shorter wavelength may be regarded as a consequence of the enhanced photon absorption and shortened lifetime of the electron–hole pairs at or near the surface region of the NWs [42].

The photoresponse of the individual $SnO_2$NW-based photodetector to pulsed UV light illumination was also examined. In this measurement, the pulsed UV light source was generated by chopping the monochromatic UV light which was produced by a helium lamp attached with a monochromator, and the fast-varying signal was collected by the oscilloscope system. Figure 6(b) depicts the reversible switching of the $SnO_2$NW photodetector between high and low conductance when the UV light was turned on and off. The response is fast and exhibits long-term repeatability in the range from 100 to 500 Hz. Further study of the dark current as a function of chopping frequency reveals a slow relative balance ($(I_{max} - I_{min})/I_{max}$) decay. The relative balance remained larger than 82% even when the frequency

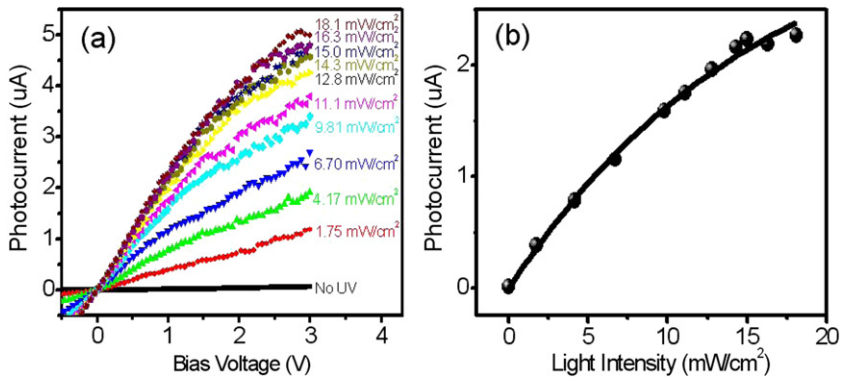


**Figure 7.** (a) $I$–$V$ curves of a single $SnO_2$NW-based photodetector under UV light illumination with intensity in the range from 0 to 18.1 mW $cm^{-2}$. (b) Fitting curve of the relationship between the light intensity and the photocurrent at a bias voltage of 1 V (incident light wavelength: 320 nm).

**Table 1.** Summary of relative balance and rise time/fall time of photodetectors fabricated from different kinds of semiconductor nanostructures.

| | Relative balance/ frequency (Hz) | Rise time/fall time (ms) | Reference |
|---|---|---|---|
| $SnO_2$ nanowire | 82%/500 | 0.21/0.30 | Our work |
| ZnO nanowire | — | 0.20/0.50 | [24] |
| GaN nanowire | — | 1000–2000/>120 000 | [25] |
| ZnS nanowire | 20%/100 | 46 000/30 000 | [41] |
| CdS nanoribbon | 77%/500 | 0.746/0.794 | [42] |
| CdSe nanoribbon | 40%/400 | 0.639/5.86 | [43] |
| Se nanowire | 76%/500 | 0.40/1.23 | [44] |

was increased to 500 Hz. To the best of our knowledge, this is the highest value found, compared with reported values available (cf table 1). With reference to response speed (the time required to increase the photocurrent from 10 to 90% of the peak value or vice versa is defined as the rise time or the fall time, respectively), a rise/fall time of 0.42 ms/0.60 ms was obtained. This response speed is comparable with a UV photodetector made from ZnO nanowire [25], but much quicker than devices made from GaN [26] and ZnS nanowires [43], and visible light photodetectors made from CdS [44], CdSe [45], and Se nanostructures (table 1) [46]. Two factors are responsible for the relatively fast photoresponse. (1) Small size effect. As observed in CdSe and Se NWs, owing to the large surface-to-volume ratio, the abundant quantity of vacancies or dangling bonds on the NW surfaces can function as recombination centers, which will facilitate the recombination process of photocarriers [43, 44]. (2) High-quality crystallinity of the $SnO_2$NWs. The NWs obtained via this approach are single crystal and free of defects in their interior parts. Such a structural feature will accelerate the achievement of steady state for photocurrent at both the rise and the fall stages.

The photoresponse of the $SnO_2$NW based photodetector depends on the illumination power as well. As exhibited in figure 7(a), the photocurrent of the $SnO_2$NW increases gradually with increase of the radiation intensity. The relationship between the photocurrent ($I$) and light intensity ($P$) can be described by a simple power law: $I = aP^b$, where $a$ is a proportionality constant associated with the light wavelength, and the exponent $b$ is another constant that relates device response to light intensity. By fitting this formula to the experimental data, we obtained $b = 0.821$ for the 320 nm light [39]. The noninteger exponent can be regarded as a consequence of the complex process of electron–hole generation, trapping and recombination within the $SnO_2$NWs. Further similar fitting gives $b = 0.817$ and 0.805 for 310 and 290 nm light, respectively. These identical values for different wavelengths suggest that the photoresponse of our $SnO_2$NW based photodetector is wavelength independent.

## 4. Conclusions

In summary, we demonstrated the Sn-catalyzed fabrication of $SnO_2$NWs via a VLS process, in which Sn nanoparticles can direct the oriented growth. $SnO_2$NW-based FET characterization revealed typical n-type conduction, with a carrier mobility and concentration of 14.36 $cm^2$ $V^{-1}$ $s^{-1}$ and $1.145 \times 10^{17}$ $cm^{-3}$, respectively. Further photoconductive analysis showed that the as-prepared $SnO_2$NW-based photodetector exhibits a high photo-to-dark current ratio of three orders of magnitude at 320 nm, and can function with excellent reproducibility, stability and high response speed (rise/fall time of 0.42 ms/0.60 ms) in a wide range of chopping frequencies. The totality of the above results suggests that the $SnO_2$NWs obtained via this approach can be employed to develop a high-performance UV light photodetector.

## Acknowledgments

The authors acknowledge the financial support from the Start-up Fund of Hefei University of Technology, the National Natural Science Foundation of China (Nos 60806028 and 21101051), the Program for New Century Excellent Talents in University of the Chinese Ministry of Education (NCET-08-0764), the Major Research Plan of the National Natural Science Foundation of China (No. 91027021), and the Fundamental Research Funds for the Central Universities.

## References

[1] Yang R S and Wang Z L 2006 *J. Am. Chem. Soc.* **128** 1466
[2] Lieber C M 2003 *MRS Bull.* **28** 486
[3] Hu J Q, Bando Y, Liu Q L and Golberg D 2003 *Adv. Funct. Mater.* **13** 493
[4] Pan Z W, Dai Z R and Wang Z L 2001 *Science* **291** 1947
[5] Fraigi L B, Lamas D G and De Reca N E W 2001 *Mater. Lett.* **47** 262
[6] Nguyen P, Ng H T, Yamada T, Smith M K, Li J, Han J and Meyyappan M 2004 *Nano Lett.* **4** 651
[7] Huang M H, Mao S, Feick H, Yan H, Wu Y, Kind H, Weber E, Russo R and Yang P D 2001 *Science* **292** 1897
[8] Chang K W and Wu J. J 2004 *Adv. Mater.* **16** 545
[9] Liu Y, Dong J and Liu M L 2004 *Adv. Mater.* **16** 353
[10] Yang F and Forrest S R 2006 *Adv. Mater.* **18** 2018
[11] Okuya M, Kaneko S, Hiroshima K, Yagi I and Murakami K 2001 *J. Eur. Ceram. Soc.* **21** 2099
[12] Lee J H, Yezerets A, Kung M C and Kung H H 2001 *Chem. Commun.* **15** 1404
[13] Dong Q, Su H L, Zhang D and Zhang F Y 2006 *Nanotechnology* **17** 3968
[14] Choe Y S, Chung J K, Kim D S and Baik H K 1999 *Thin Solid Film* **341** 230
[15] Jeong J, Choi S P, Chang C I, Shin D C, Park J S, Lee B T, Park Y J and Song H J 2003 *Solid State Commun.* **127** 595
[16] Chen Z W, Jiao Z, Wu M H, Shek C H, Wu C M L and Lai J K L 2009 *Mater. Chem. Phys.* **115** 660
[17] Zhu J J, Lu Z H, Aruna S T, Aubach D and Gedanken A 2000 *Chem. Mater.* **12** 2557
[18] Zhang R Q, Lifshitz Y and Lee S T 2003 *Adv. Mater.* **15** 635
[19] Wang W W, Zhu Y J and Xia Y L 2007 *Adv. Funct. Mater.* **17** 59
[20] Sun S H, Meng G W, Zhang G X, Masse J P and Zhang L D 2007 *Chem.—Eur. J.* **13** 32
[21] Kolmakov A, Zhang Y X, Cheng G S and Moskovits M 2003 *Adv. Mater.* **15** 997
[22] Law H K, Messer B, Kim F and Yang P D 2002 *Angew. Chem. Int. Edn* **41** 2405
[23] Wang H, Xu J Q and Pan Q Y 2010 *CrystEngComm* **12** 1280
[24] Law J B K and Thong J T L 2006 *Appl. Phys. Lett.* **88** 133114
[25] Calarco R, Marso M, Richter T, Aykanat A I, Meijers R, Van der Hart A, Stoica T and Lüth H 2005 *Nano Lett.* **5** 981
[26] Freitag M, Martin Y, Misewich J A, Martel R and Avouris P 2003 *Nano Lett.* **3** 1067
[27] Wan Q, Dattoli E and Lu W 2008 *Small* **4** 451
[28] Kim D, Kim Y K, Kim S C, Ha J S, Huh J, Na J and Kim G T 2009 *Appl. Phys. Lett.* **95** 043107
[29] Hu L F, Yan J, Liao M Y, Wu L M and Fang X S 2011 *Small* **7** 1012
[30] Cheng L, Shao M W, Chen D Y, Ma D D D and Lee S T 2010 *CrystEngComm* **12** 1536
[31] Hu J Q, Bando Y and Golberg D 2003 *Chem. Phys. Lett.* **372** 758
[32] Jo Y H, Jung I, Choi C S, Kim I and Lee H M 2011 *Nanotechnology* **22** 225701
[33] Hu J Q, Ma X L, Shang N G, Xie Z Y, Wong N B, Lee C S and Lee S T 2002 *J. Phys. Chem.* B **106** 3823
[34] Gao P X, Ding Y and Wang Z L 2003 *Nano Lett.* **3** 1315
[35] Wu P, Zou X Q, Chi L F, Li Q and Xiao T 2007 *Nanotechnology* **18** 125601
[36] Rathi S J, Jariwala B N, Beach J D, Stradins P, Taylor P C, Weng X J, Ke Y, Redwing J M, Agarwal S and Collins R T 2011 *J. Phys. Chem.* C **115** 3833
[37] Yu L W, Alet P J, Picardi G, Maurin I and Cabarrocas P R 2008 *Nanotechnology* **19** 485605
[38] Barin I I 1995 *Thermochemical Date of Pure Substances* 3rd edn (New York: VCH)
[39] Liu Z Q, Zhang D H, Han S, Li C, Tang T, Jin W, Liu X L, Lei B and Zhou C W 2003 *Adv. Mater.* **15** 1754
[40] Ma R M, Dai L and Qin G G 2007 *Nano Lett.* **7** 868
[41] Rose A 1978 *Concepts in Photoconductivity and Allied Problems* (New York: Krieger)
[42] Amalnerkar D P 1999 *Mater. Chem. Phys.* **60** 1
[43] Yu Y Q *et al* 2011 *J. Mater. Chem.* **21** 12632
[44] Jie J S, Zhang W J, Jiang Y, Meng X M, Li Y Q and Lee S T 2006 *Nano Lett.* **6** 1887
[45] Jiang Y, Zhang W J, Jie J S, Meng X M, Fan X and Lee S T 2007 *Adv. Funct. Mater.* **17** 1795
[46] Luo L B, Jie J S, Chen Z H, Zhang X J, Fan X, Yuan G D, He Z B, Zhang W F, Zhang W J and Lee S T 2009 *J. Nanosci. Nanotechnol.* **9** 6292